Ⓔ

THREE-DIMENSIONAL MAGNETOHYDRODYNAMIC SIMULATION OF A GLOBAL SOLAR CORONA USING A TEMPERATURE DISTRIBUTION MAP OBTAINED FROM *SOHO* EIT MEASUREMENTS

KEIJI HAYASHI, ELENA BENEVOLENSKAYA, TODD HOEKSEMA, YANG LIU, AND XUE PU ZHAO
W. W. Hansen Experimental Physics Laboratory, Stanford University, 445 Via Palou, Stanford, CA 94305; keiji@quake.stanford.edu

ABSTRACT

The temperature at the base of the solar corona is one of the important factors in determining the solar coronal structure. In this Letter, we performed the time-dependent magnetohydrodynamic (MHD) simulation for the solar corona utilizing the temperature map derived from the multiwavelength observation by the EUV Imaging Telescope (EIT) on the *Solar and Heliospheric Observatory* (*SOHO*) and the magnetic field map from the Michelson Doppler Imager (MDI) on *SOHO*. We analyzed the difference in three-dimensional magnetic field topology obtained when the uniform base temperature adopted in standard simulations is replaced by the observation-based, nonuniform temperature distribution. The differences in the magnetic field topology obtained as the response of the solar corona to the changes of the temperature at the coronal base depict the role of the plasma conditions at the coronal base in the dynamics of the global solar corona. This work is our first effort to utilize the data of the solar coronal plasma as the boundary condition to enhance the MHD simulations of a solar corona.

Subject headings: methods: numerical — MHD — solar wind — Sun: corona

Online material: color figures

1. INTRODUCTION

The time-dependent MHD simulation is widely used to retrieve the trans-Alfvénic solar coronal structures. In this kind of MHD simulation, the photospheric magnetic field measurement data has been widely used as the boundary values on the inner boundary sphere to specify the simulated situation and period.

Because the solar coronal structure is determined as the consequence of the nonlinear MHD process, the boundary values of the plasma parameters are also decisive factors in the simulation of the solar corona. For example, the higher temperature at the coronal base generates greater gas pressure that may either inflate the closed field structure or open the magnetic field at the outer parts of the streamer that could be closed with lower base temperature. The general tendency of whether the coronal magnetic field can be closed or open has been discussed (e.g., Low 1996). It is preferable if the boundary values of plasma parameters are determined from the measurement data. In many simulation studies, however, uniform plasma distribution on the solar surface has been assumed to start the simulation.

With the CHIANTI software (e.g., Dere et al. 1997; Young et al. 2003), we can calculate the coronal temperature from the multiwavelength observations by the *SOHO* EIT. Such available observation-based temperature data will help to describe the simulated situation much more realistically. In addition, the EIT measurement temperature map allows us to avoid considering unknown processes or assuming models of coronal heating, because the EIT observation-based temperature represents the consequence of the complex and unknown processes at the lower corona.

We have recently developed the time-dependent MHD simulation code for the solar corona (Hayashi 2005). Our code contains the boundary treatment that is based on the concept of the projected normal characteristics method (Nakagawa et al. 1987; Wu & Wang 1987). This boundary treatment can avoid the mathematical and physical inconsistency of the fixed boundary conditions posed on the sub-Alfvénic boundary. With this feature, the simulated three-dimensional MHD variables fully match the given boundary conditions, and the numerical solutions of the steady state of the solar corona do not have numerical oscillation near the sub-Alfvénic inner boundary surface.

In this study, as our first effort to utilize the observation-based coronal plasma parameters as the constraint of an MHD simulation, we performed the MHD simulation of a solar corona using the boundary temperature map obtained from *SOHO* EIT multiwavelength measurements and the magnetic field map obtained from *SOHO* MDI measurements. The obtained magnetic field structure of the simulated solar corona is compared to that simulated with the synthetic uniform temperature, in order to examine how the observation-based temperature influences the simulated solar corona.

2. METHOD AND DATA

In order to simulate the solar corona with the observation-based temperature map and the synthetic uniform one, we performed a three-step simulation. In the first simulation step, the synthetic uniform temperature of 1.4 MK is given as the fixed boundary value on the inner boundary sphere. The steady quiet corona matching this uniform temperature distribution is obtained as the time-relaxed solution of the three-dimensional time-dependent MHD simulation. In the second step, then, the temperature on the inner boundary is changed gradually until the boundary temperature becomes identical to the EIT-based temperature map. In the last step, the time-relaxation simulation is continued until the system reaches a new steady state. The total simulated time was about 90 hr in physical time: 40 hr for the first step, 10 hr for the second step, and 40 hr for the last step. These times are sufficient to obtain the time-relaxed state of the solar corona.

Through the second and third simulation, the differences between the quiet corona with a synthetic uniform temperature map and with the observation-based temperature map are obtained as the response of the simulated system to the change of the boundary temperature.

2.1. *Boundary Maps of Temperature and Magnetic Field*

We chose the period of Carrington rotation (CR) 2006, in 2003 August. This period corresponds to the early part of the declining phase of the solar activity cycle; thus, there were a variety of coronal structures, such as active regions and coronal holes. We used the algorithm by Zhang et al. (1999) with the CHIANTI software to determine the boundary temperature map. The low- and high-temperature components can be evaluated. We used the average of the two components, whose distribution is shown in Figure 1a. To fill the data gaps at the southern pole region and remove data discontinuities, this temperature map is smoothed in terms of a Gaussian with a half-width of $7°.5$ at the equator and $15°$ at the pole. The smoothed temperature map ranges from 1.21 to 2.04 MK. In this study, to prevent the coronal material falling when the imposed temperature is lower than the synthetic one, the temperature less than 1.4 MK is reset to 1.4 MK. Figure 1b shows the temperature distribution determined in this way.

We chose 1.15 $R_\odot$ as the heliocentric distance of the inner boundary sphere, because an EIT temperature map may best represent the temperature there. To start the simulation, therefore, we have to determine the boundary distribution of the magnetic field distribution of 1.15 $R_\odot$. In this study, the magnetic field boundary map is calculated with the source surface-potential field model (Schatten et al. 1969) in terms of the spherical harmonics polynomial up to the seventh term. The magnetic field at lower corona and active regions may have substantial nonpotentiality, although the potential field model with this coefficient number well describes the global coronal magnetic field. We used the photospheric magnetic field data obtained from *SOHO* MDI measurement data for the period CR 2006. Figure 1c shows the map of the radial component of the boundary magnetic field at 1.15 $R_\odot$ determined in this way. The radial component of the boundary magnetic field is fixed all through the three-step simulation.

2.2. *MHD Simulation Code*

The identical simulation code is used in all three simulation steps. The governing equations of the system are the time-dependent MHD equations. Most parts of the MHD code are the same as described by Hayashi (2005); the two-step explicit TVD-MUSCL method with third-order spatial accuracy is used to trace the temporal evolutions of MHD variables, and the treatment of the inner sub-Alfvénic boundary is based on the projected normal characteristic method.

The simulation grid points are constructed in the spherical coordinate system so that the input temperature and magnetic field map is used directly without modification. The simulation region is between the two heliocentric spheres: the inner boundary sphere at 1.15 $R_\odot$ on which the observational data is posed and the upper boundary sphere at 30 $R_\odot$ on which the solar wind is always super-Alfvénic. Both latitudinal and longitudinal angular size of the cell volume is set at uniformly $2°.8$.

The polytropic gas with specific heat ratio $\gamma = 1.05$ is assumed in the computational domain at $r > 1.15\ R_\odot$ to mimic
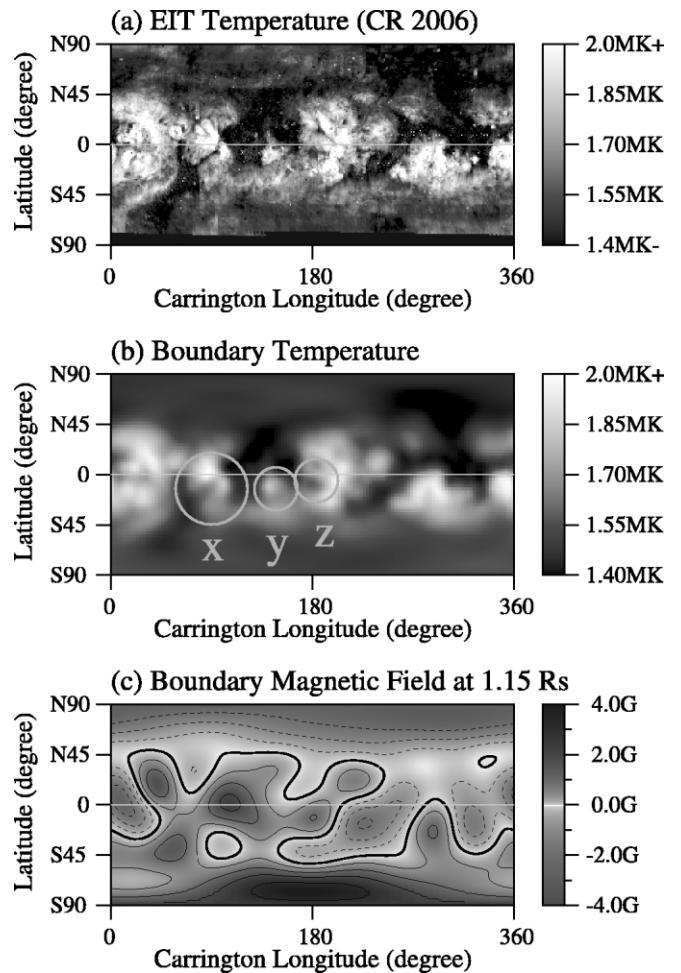

Fig. 1.—Boundary maps at 1.15 $R_\odot$. (*a*) The temperature map obtained from the EIT emission ratios. (*b*, *c*) The smoothed temperature and the magnetic field map imposed on the inner boundary sphere at 1.15 $R_\odot$, respectively. The solid and dashed contour lines in (*c*) are made with the interval of 1 G for positive and negative polarity, respectively. The circles—x, y, and z—highlight the regions discussed in the text. [*See the electronic edition of the Journal for a color version of this figure.*]

the high thermal conductivity and produce the trans-Alfvénic solar wind. On the inner boundary at $r = 1.15\ R_\odot$, the boundary treatment in our code updates the gas pressure and mass density on the inner boundary surface preserving the local given temperature during the time increment simulation step.

In this study, the first simulation step is started with the uniform plasma density distribution, with number density of $5 \times 10^7\ \mathrm{cm}^{-3}$ at 1.15 $R_\odot$. The boundary treatment based on the projected normal characteristic method produces the density contrast that matches the given temperature and magnetic field distribution maps and satisfies the nonlinear hyperbolic MHD equation system.

3. RESULTS

The magnetic field lines are a good proxy to examine the differences between the cases with a uniform temperature map and that of the observation-based map. Figure 2 shows the coronal magnetic field lines and the surface plasma parameters in the steady state at the first and third step of the time-relaxation MHD simulation. Figure 2a demonstrates the closed field lines in the steady state at the first simulation step with a uniform
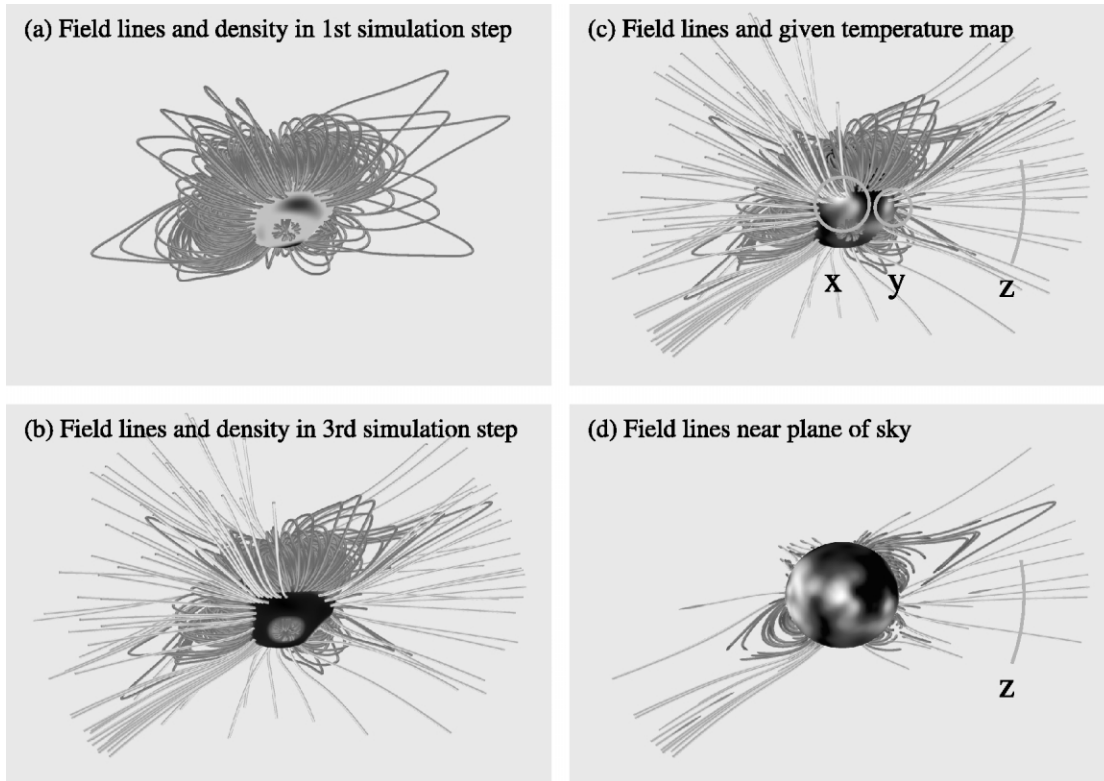
Fig. 2.—Field lines and boundary plasma parameters. The closed field lines obtained in the first simulation step are drawn in (*a*). The field lines obtained with the third simulation step are drawn in (*b*) and *c*), with the brighter lines showing the newly open lines. The brightness on the sphere in (*a*) and (*b*) shows the density at 1.15 $R_\odot$, and the brightness in (*c*) shows the given temperature. The field lines and solar surface plasma are viewed from the direction of Carrington longitude of 90° and the heliographic latitude of 6°.5 north that approximately corresponds to Earth's position on 2003 August 22, 21:00 UT. [*See the electronic edition of the Journal for a color version of this figure.*]

boundary temperature. Figures 2*b*, 2*c*, and 2*d* show the field lines in steady state at the third step; the brighter lines are the magnetic field lines that were closed in the first step but open in the third simulation step. Thus, the brighter lines best represent the response of the coronal magnetic field structure to the change of the temperature imposed on the coronal base. The field lines drawn in Figure 2*c* are identical to that in Figure 2*b*, and only the lines that passed near the plane of sky are drawn in Figure 2*d*. The brightness on the inner boundary sphere in Figures 2*a* and 2*b* shows the density obtained on the inner boundary sphere at 1.15 $R_\odot$, and the imposed temperatures are shown with the brightness in Figures 2*c* and 2*d*.

A notable change of the coronal field lines is that the field lines at the outermost part of the closed field regions became open to the interplanetary space. The change of magnetic field topology is significant especially when the high-temperature regions, such as active regions, locate near the coronal hole. The circles x and y in Figure 2*c* highlight such newly open field lines at high-temperature regions. The circles in Figure 1 show the corresponding positions.

The arc (z) in Figure 2*d* highlights another notable change of the coronal magnetic field structure, showing the latitudinal range of the newly open field region. Because the imposed temperature at the base of this newly open field region (marked circle z in Fig. 1) was lower than the surrounding regions, the newly opened field lines (z) are thought to be induced by the inflation of the neighboring streamer. Therefore, this case shows the plasma condition at the neighboring regions can influence the tendency of whether the coronal magnetic field could be open or closed. It should be mentioned here that the relationship

between the coronal magnetic field topology and the nonuniform observation-based plasma distribution at the coronal base can be first examined by solving the nonlinear MHD equation with the time-dependent three-dimensional MHD simulations.

Figure 3 is the superimposed disk image of the *SOHO* Large Angle and Spectrometric Coronagraph (LASCO) C2 and EIT 284 of 2003 August 22, to which the viewing point of plots in Figure 2 correspond. The arc (z) in Figure 3 shows the latitudinal range identical to that shown in Figures 2*c* and 2*d*. Because of the presence of the relatively large coronal holes (marked with "CH" in Fig. 3) and because of the complexity of the structure at the actual lower corona, it is difficult to identify which coronal structure at low altitude is the base of the dark regions (z). However, the dark region (z) persisted before and after a few days, and its position well coincides with the simulated newly open field region. Therefore, this simulation with observation-based temperature distribution might successfully retrieve some structure that could not be obtained with the synthetic uniform temperature map.

4. DISCUSSION

A three-step MHD simulation of the solar corona is performed to compute the steady state of the solar corona with the synthetic uniform temperature map and with the observation-based temperature map. By starting the simulation from 1.15 $R_\odot$, we can avoid the unknown mechanism at the active region and lower corona and directly utilize the observation data representing the consequences of the unknown mechanism. Although the simu-
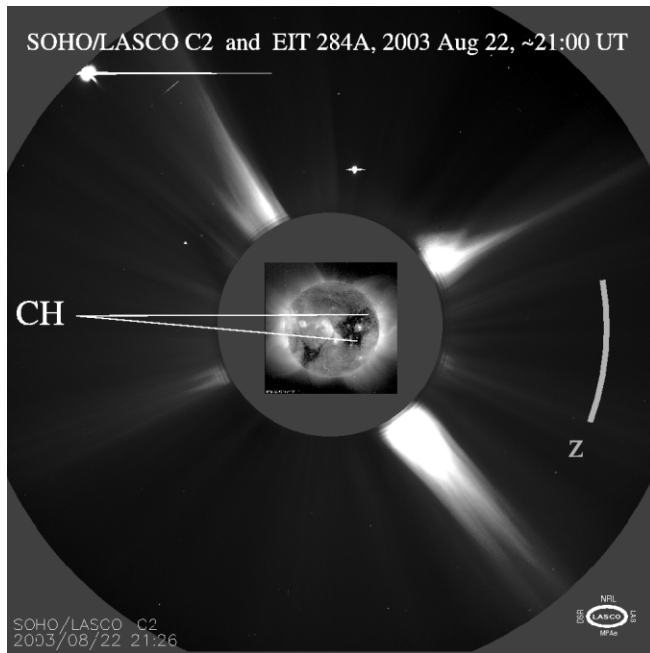
FIG. 3.—*SOHO* LASCO C2 and EIT 284 image data of 2003 August 22, around 21:00 UT. [*See the electronic edition of the Journal for a color version of this figure.*]

lation including such dynamics is desirable, this feature allows the simple description of the simulated situation.

The steady coronal magnetic field structures of these two cases are compared. The newly open field structures are mostly found at the regions where the base temperature increased.

Because the temperature at the base of the solar corona is a good proxy of the intensity of the small-scale solar surface activities, such as magnetic reconnection and Alfvén wave decay, the differences of the two simulation cases show a process through which the spatial distribution and temporal evolution of the small-scale solar surface activities determine the large-scale structure of the solar corona in terms of the pressure balance.

In this simulation, the density distribution is an output of the simulation. As demonstrated in Figures 2*a* and 2*b*, the obtained distribution of the plasma density is reasonable; the low-density regions form at the simulated open field regions that coincide well with the dark region observed by LASCO C2. Because of a lack of data, we did not quantitatively check the simulated density distribution at 1.15 $R_\odot$. It should be mentioned here that if the density distribution map is available, our simulation model can use it as the input boundary data in a manner similar to that used in this study for the temperature map.

REFERENCES

Dere, K. P., et al. 1997, A&AS, 125, 149
Hayashi, K. 2005, ApJS, 161, 480
Low, B. C. 1996, Sol. Phys., 167, 217
Nakagawa, Y., Hu, Y. Q., & Wu, S. T. 1987, A&A, 179, 354
Schatten, K. H., Wilcox, J. M., & Ness, N.F. 1969, Sol. Phys., 6, 442
Wu, S. T., & Wang, J. F. 1987, Comput. Methods Appl. Mech. Engineering, 64, 267
Young, P. R., et al. 2003, ApJS, 144, 135
Zhang, J., White, S. M., & Kundu, M. R. 1999, ApJ, 527, 977